J. Fluid Mech. (1983), *vol.* 126, *pp.* 91–121
Printed in Great Britain

Multicellular natural convection in a vertical slot

By YEE LEE† AND SEPPO A. KORPELA
Department of Mechanical Engineering, The Ohio State University, Columbus, Ohio 43210

(Received 13 October 1981 and in revised form 29 July 1982)

In this article we present numerical solutions to multicellular natural convection in a vertical enclosure. The calculated streamlines faithfully represent what has been seen in the laboratory by smoke traces in air and particle traces in oils. The calculated isotherms for air correspond to reported interferometric patterns. Solutions exhibiting travelling waves for water were calculated near conditions where they should occur according to linear stability theory. Heat-transfer results for air are given and their dependence on the aspect ratio of the enclosure exhibited.

1. Introduction

Natural convection in a vertical cavity has been under study for the past seventy years. The practical aim of the effort has been to relate the heat transfer across the cavity to the temperature difference between the vertical sidewalls. The direct way to accomplish this is to build a laboratory apparatus and measure the heat transfer. Many experiments of this sort were carried out during the early part of this century, and the heat-transfer correlations so obtained can still be found in textbooks. They have served the design engineer adequately throughout the years.

Average heat-transfer measurements did not, however, elucidate the structure of the flow. To gain a deeper understanding of convection, local measurements and theoretical ideas were needed. Eckert & Carlson (1961) and Elder (1965) showed in experiments the form of the temperature and velocity fields, and, on the basis of these, the early theoretical ideas of Batchelor (1954) could be refined by Elder (1965) and Gill (1966), so that the main features of the flow are understood today.

The elementary aspects of the flow are obvious to anyone who knows that hot fluid rises and cold fluid sinks. For then in a closed cavity the fluid is expected to flow up near the hot boundary, turn in the top end, sink near the cold wall to the bottom, and there turn again to complete a cycle. With further thought one becomes convinced that, provided the fluid properties are constant, this flow is symmetrical about the centre of the cavity. This can be tested by writing the equations governing the flow and investigating their symmetry properties. The particular symmetrical state of the flow is of course determined by the numerical values of the parameters of the equations. If the equations have been put into a non-dimensional form, it becomes clear that there are only three independent parameters that describe the flow. These are the Rayleigh number $R = g\beta\Delta TL^3/\alpha\nu$, the Prandtl number $P = \nu/\alpha$, and the aspect ratio $H = l/L$. The symbols used to define the parameters are the conventional ones, with l being the height of the cavity and L its width.

The aim of theoretical research is to see how the governing equations can be simplified as these parameters assume certain limiting values. With three non-dimensional groups present a number of limits can be taken. Batchelor (1954)

† Present address: Technical Center, Owens–Corning Fiberglas, Granville, Ohio 43023.

considered three of them. For a fixed R he examined the flow as $H \to \infty$, and for a fixed H the limits $R \to 0$ and $R \to \infty$. In the first case he showed that in the centre region the flow is parallel and heat is transferred across the cavity mainly by conduction. This regime of flow has come to be called the conduction regime. To be sure, across the ends heat is also convected, but the terminology is useful in classifying the flows. The temperature distribution across the midheight of the cavity in this flow is linear, which in turn leads to a cubic for the vertical velocity.

The limit of fixed H and $R \to \infty$ leads to emergence of boundary layers on the vertical sidewalls and a core in the centre. In this, the so-called boundary-layer regime, heat is transferred primarily by horizontal convection across the ends. The flow in the ends is, however, sufficiently complex that the analysis of the flow in the boundary-layer regime is still incomplete today.

For intermediate values of Rayleigh number the flow is said to be in the transition regime. By using a Mach–Zehnder interferometer, Eckert & Carlson (1961) established that, except in the conduction regime, the core in the centre becomes stably stratified, meaning that temperature increases with height. Near the midheight the rise is linear. Using this fact and assuming that the horizontal velocity is zero, Elder (1965) calculated the vertical velocity and the temperature profiles near the midheight. The profiles have the proper shape and magnitude if the vertical temperature gradient, which is a parameter in his equations, is adjusted to fit the experimental data.

Gill (1966), at about the same time, constructed a boundary-layer theory of the flow. However, he was not able to match the boundary layers to the flow conditions in the end regions. No simplification of the equations has been found that would allow analytical solutions to be obtained in the region where the flow turns around. Gill used the condition that the top and bottom are impermeable to complete his analysis. This has been modified by Bejan (1979), who instead required that the vertical heat flux in the ends be zero. The heat-transfer correlation derived on this basis is reasonably close to many of the experiments and machine computations, but on a logarithmic plot its slope is a bit too low. In their studies Gill and Bejan assumed the Prandtl number to be large. Recently Graebel (1980) carried out the analysis where this need not be so.

During the past twenty years machine calculations have become a viable alternative to study fluid flow. In this period the power of digital computers to perform arithmetic operations has increased greatly, and better algorithms have been invented as well. We mention the studies of Wilkes & Churchill (1966), Elder (1966), de Vahl Davis (1968), Rubel & Landis (1969), and Newell & Schmidt (1970), which give finite-difference solutions for natural convection in a vertical cavity, each extending the range of the computations to higher values of Rayleigh number and aspect ratio than was possible previously. In the next decade many more studies were completed. Of these the work of Quon (1972, 1977) is notable. He gives a lucid account of the boundary-layer regime in a square cavity, confirming as others had noted before him, that the flow changes little with Prandtl number as long as the Prandtl number is greater than about seven. Of interest also is his observation that a stress-free top boundary alters the flow neither in the vertical layers nor in the core. The horizontal velocity is affected in a region near the top, the thickness of which is about a sixth of the total height of the cavity, but the temperature even here remains unaffected. These results are consistent with the structure of Gill's solution, which shows that each vertical boundary layer entrains fluid in its upstream half and ejects it in the downstream half. While crossing the core the temperature of the fluid does not change. Quon's solution shows this to be true also in the end regions. The entrainment had

been suggested by Elder to be responsible for the stably stratified thermal structure of the core.

Other studies include that of Roux *et al.* (1978), one by Küblbeck, Merker & Straub (1980) and the work of Lauriat (1980). In the first two the authors investigate flows in a square cavity. Roux *et al.* use a fourth-order Hermitian method which puts the finite-difference equations into a block-tridiagonal form allowing for their rapid solution. Küblbeck *et al.*, on the other hand, obtain high accuracy by non-uniform grids through coordinate stretching, and show in detail in their paper the time evolution of the flow. Lauriat investigated four different numerical schemes for convection in a cavity of aspect ratio 10. These papers add little new physical insight to the flow.

In addition to providing the basis for understanding the flow in the boundary-layer and transition regimes, Elder's (1965) experiments opened another avenue for research; namely, the study of stability of the vertical shear flow. He observed multicellular convection in the cavity, attributable to hydrodynamic instability. Actually, although unknown in the West, Gershuni (1953) in Russia had already attempted to calculate the stability of the flow in the conduction regime. More-accurate calculations came later (Rudakov 1967; Birikh *et al.* 1972, Korpela, Gözüm & Baxi 1973; Ruth 1979). Stability calculations of the flow in the transition and boundary-layer regimes appeared also (Gill & Davey 1969; Gill & Kirkham 1970; Hart 1971; Bergholz 1978).

What is known now is that at low Prandtl numbers for tall cavities steady multicellular convection appears at sufficiently high Rayleigh numbers. Vest & Arpaci (1969) observed this in the laboratory for air in a cavity of aspect ratio 33. For high-Prandtl-number fluids in very tall cavities two waves appear at the onset of instability. They propagate in opposite halves of the cavity in the direction of the base flow. To see these in the laboratory one would need to build a cavity that is several hundred times taller than it is wide. Nobody has undertaken to do this.

Bergholz's contribution was to show that the travelling-wave solutions arise also from the instability of the transition and boundary-layer regimes, and that they are present for low-Prandtl-number fluids in cavities the aspect ratio of which is only moderately large. Recently Schinkel (1980) observed these waves in interferograms for air in cavities of aspect ratios ranging from 5 to 9. Bergholz also showed that the onset of instability for high-Prandtl-number fluids can in turn set in through stationary states. It is, in fact, exactly in this situation in which Elder originally observed the multicellular flow. He used oil with $P = 1000$ in a cavity with an aspect ratio in the range from 12 to 60.

In a few studies the flow after the onset of instability has been calculated numerically. Thomas & de Vahl Davis (1970) did this for a flow in an annular cavity of aspect ratio 25 and ratio of the inner to outer radius equal to $\frac{2}{3}$. They obtained a solution with five cells in a fluid with Prandtl number equal to unity. Pepper & Harris (1977) did similar calculations for annuli of aspect ratio 5 and radius ratios $\frac{1}{3}$ and $\frac{1}{2}$, for a fluid with $P = 1$. In reading their paper one soon notes that the contour plots they present have been printed upside down, and as they are they would, in fact, represent the situation in which the outer wall is heated. Their calculated Nusselt numbers are in good agreement with the results of Thomas & de Vahl Davis. When they increase the aspect ratio of the annulus to 15, while keeping the radius ratio at $\frac{1}{2}$, their stream patterns show wiggles which could indicate boundary-layer instability on the top part of the annulus. The oscillations could also be the result of inadequate resolution. We have shown by calculations that multicellular convection takes place at the condition in which Thomas & de Vahl Davis obtained it. The

multicellular structure, however, is one of upward-drifting cells making the flow periodic in time (Choi & Korpela 1980; Lee, Korpela & Horne 1982).

Pepper & Harris also consider the flow of a high-Prandtl-number fluid in a rectangular cavity of aspect ratio 10. In this case they saw a three-cell structure in the centre of the cavity. This had already been calculated earlier by de Vahl Davis & Mallinson (1975), and their results represent Elder's observations very faithfully, including the so-called tertiary cells visible in the experiments. A similar calculation and further experiments by Seki, Fukusako & Inaba (1978) confirm the structure of the flow at high Prandtl numbers. For air Grondin & Roux (1979) show the existence of multicellular convection in a cavity of aspect ratio 16.

Three-dimensional calculations have been carried out by Mallinson & de Vahl Davis (1973, 1977) as well as by Ozoe (1976) and Ozoe *et al.* (1978). Although in experiments the heat transfer has been found to be independent of the depth of the cavity, as long as the depth is not too small, the numerical calculations show the flow to be certainly three-dimensional. The reason for this is that the rotating core flow induces something like an Ekman layer on the end walls of a cubical box. The features seen in the numerical calculations have now also been observed in the laboratory (Morrison & Tran 1978).

In the following sections we present results of numerical calculations of the multicellular flow. Such flows occur only in cavities of large aspect ratio. Most of the numerical studies to date have been for cavities with aspect ratios less than ten. Except for liquid metals, for which we have found the multicellular structure to emerge when the aspect ratio is as low as six, for air the aspect ratio must be at least 12 before the flow changes to a more-complex structure as a result of instability. Our most complete results are for air because of its importance in the design of doublepane windows. It was, in fact, this application that originally motivated Batchelor (1954) to study this flow. We have also found some travelling-wave solutions for water and essentially reproduced the results of de Vahl Davis & Mallinson when $P = 1000$.

2. Formulation

Consider a vertical rectangular cavity of height l and width L as shown in figure 1. The left sidewall is held at the temperature T_1, which is higher than the temperature T_2 of the right wall. The top and bottom of the cavity are insulated. A Newtonian fluid of density ρ, kinematic viscosity ν and thermal diffusivity α is contained in the cavity. The equations governing the flow and heat transfer can be put into non-dimensional forms by scaling the width of the cavity by L, its height by l, time by L^2/ν, temperature by $\Delta T = T_1 - T_2$, and velocities and pressure by U and ρU^2 respectively. Here $U = g\beta\Delta T L^2/\nu$ is the characteristic thermal velocity obtained by balancing the viscous shear force with the buoyant force. In the expression for the buoyancy β is the volumetric coefficient of thermal expansion and g the gravitational acceleration. Assuming further that density changes are important only in the gravitational term and that the temperature T is measured above the temperature of the cold wall, the governing equations become,

$$\nabla . \mathbf{q} = 0, \tag{1}$$

$$\frac{\partial \mathbf{q}}{\partial t} + G(\mathbf{q} . \nabla)\,\mathbf{q} = -G\nabla p + T\mathbf{j} + \nabla^2 \mathbf{q}, \tag{2}$$

$$\frac{\partial T}{\partial t} + G(\mathbf{q} . \nabla)\,T = \frac{1}{P}\nabla^2 T, \tag{3}$$

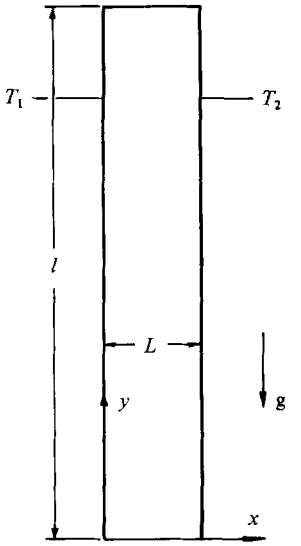

FIGURE 1. A sketch of the vertical slot.

where the del operator is defined as

$$\nabla = \mathbf{i}\frac{\partial}{\partial x} + \mathbf{j}\frac{1}{H}\frac{\partial}{\partial y}.$$

The quantity $\mathbf{q}$ in these equations is the non-dimensional velocity and t is the dimensionless time. In addition to the Grashof number $G = UL/\nu$ and Prandtl number $P = \nu/\alpha$ which appear as parameters in these equations, the aspect ratio $H = l/L$ of the cavity enters through the definition of ∇.

The third dimension of the cavity is taken to be sufficiently large so that a two-dimensional approximation of the flow is valid. In this case it is convenient to introduce a stream function via the definition $\mathbf{q} = \nabla \times \psi\mathbf{k}$ and vorticity as $\zeta = \mathbf{k} \cdot (\nabla \times \mathbf{q})$, and then solve the vorticity and energy equation together with the Poisson equation for the stream function. That is, we seek numerical solutions to the system

$$\frac{\partial \zeta}{\partial t} = \frac{G}{H}J(\zeta, \psi) - \frac{\partial T}{\partial x} + \nabla^2\zeta, \tag{4}$$

$$\frac{\partial T}{\partial t} = \frac{G}{H}J(T, \psi) + \frac{1}{P}\nabla^2 T, \tag{5}$$

$$\nabla^2\psi = -\zeta \tag{6}$$

subject to the boundary conditions

$$\psi = \frac{\partial \psi}{\partial x} = 0, \quad T = 1 \quad \text{at} \quad x = 0,$$

$$\psi = \frac{\partial \psi}{\partial x} = 0, \quad T = 0 \quad \text{at} \quad x = 1,$$

$$\psi = \frac{\partial \psi}{\partial y} = \frac{\partial T}{\partial y} = 0 \quad \text{at} \quad y = 0 \text{ and } 1.$$

Here

$$J(\zeta, \psi) = \frac{\partial \zeta}{\partial x}\frac{\partial \psi}{\partial y} - \frac{\partial \zeta}{\partial y}\frac{\partial \psi}{\partial x}$$

is the Jacobian derivative.

To cast (4) and (5) into a finite-difference form we used the central difference for the time derivative, the method of Arakawa (1966) for the Jacobian, and the DuFort–Frankel (1953) method for the diffusive terms. Roache (1972) has pointed out that this form of differencing is well-suited for flows that exhibit hydrodynamic instabilities owing to the conservation properties of Arakawa's scheme. Festa (1970), Quon (1972), Horne & Sullivan (1974) and Wirtz & Liu (1975) have used Arakawa's method in natural-convection studies.

Because the flow domain is rectangular we could advantageously solve the Poisson equation by a direct method. The actual program we used was given to us by Professor Horne. It is based on a cyclic reduction scheme of Buneman (1969) and was written by Horne to carry out calculations of convective flows in porous media. The boundary vorticity we determined by the relation first written down by Thom (1933).

The order of accuracy of this way of solving the Boussinesq equations comes out to be between 1·85 and 1·96 when square grids are used in a square cavity. The order deteriorates somewhat when the grids are not square, which was the case in the calculations in tall cavities. The majority of the calculations we carried out with 17 grids across the cavity and up to 129 grids in the vertical direction. The time step is governed by the Courant condition $(|u_{i,j}|/\Delta x + |v_{i,j}|/H\Delta y)\, G\Delta t \leqslant 1$, and depends on the Grashof or Rayleigh number. For example, for air in a square cavity with a 33×33 grid at $R = 2000$ the time step was 1×10^{-3} and 140 steps were required to reach steady state. At $R = 100000$ we had to reduce the time step to 2×10^{-4} and required 420 steps to reach steady state using the $R = 50000$ solution as an initial condition. Since we used central differences for time the transient solution is second-order accurate in time. The computations for each time step took 0·25 ms of central-processor time per grid point on an Amdahl 470 computer.

At the onset of instability the flow for low-Prandtl-number fluids in cavities with H in the range 15–40 is in the conduction regime and the critical Grashof numbers for that reason are less than 15000. If the base flow is accurately calculated at these conditions the onset of instability should occur at the right value of Grashof number. For a fluid with Prandtl number zero our calculated velocity profiles at the midheight of a cavity of aspect ratio 15 deviate by at most 0·01 % from the cubic velocity distribution, which holds for an infinitely tall slot. The vertical velocity, in fact, departs from the cubic appreciably only in the bottom or top $\frac{1}{5}$ of the cavity. This comparison with an exact solution gives us confidence that 17 grid points also resolve the multicellular structure adequately in the horizontal direction. In the vertical direction the number of grid points was usually such that we had 10 points per cell.

As the Prandtl number is increased or the cavity has a low aspect ratio, boundary layers develop in the vertical sidewalls, and for sufficiently high Rayleigh number the boundary layers can only be resolved by increasing the number of grids near the walls in the horizontal direction. Because we could afford only a certain amount of computer time we needed to find out the maximum value of Rayleigh number for which the flow is adequately resolved by the 17 uniform grids across. To establish this we carried out a convergence study for air in a square cavity by using 9×9, 17×17 and 33×33 meshes and extrapolating the results so obtained to zero grid size. For a 17×17 mesh we found the maximum stream function to be 17 % higher than its extrapolated value at $R = 10^5$, and at $R = 10^4$ this difference was 5·9 %. The corresponding numbers for a 33×33 mesh are 4·7 % and 1·6 %.

Another measure of the accuracy of the calculations is given by the heat transfer

across the cavity. We calculated the vertically averaged Nusselt number at both walls and across each vertical plane of nodes. At steady state each of these values must agree with one another. Although the method we used to cast the Boussinesq equations to a finite-difference form is a conservative one, the calculation of the Nusselt number was not, with the result that for all meshes the maximum deviation from mean in the heat transfer occurs for planes at which the vertical velocity was the largest. For the test case on a 17×17 mesh the maximum deviation was 7 % at $R = 10^5$, this diminishing to 1 % at $R = 10^4$. By reasons of symmetry the calculation of the Nusselt number at the hot and cold walls gave identical results. Furthermore, the wall values varied less with grid size than those across any other vertical plane. We found that the vertically averaged Nusselt number calculated with a 17×17 mesh at $R = 10^5$ was 7·2 % higher than that obtained by Chu & Churchill (1977) and 8·7 % higher than that of Roux *et al.* (1978). Their results deviated 3·9 % from one another. These differences diminish to 2·6 % and 2·9 % at $R = 10^4$. For a 33×33 mesh the cited percentages reduce by slightly better than a factor of 2.

Since we are interested mainly in the onset of multicellular convection and the heat transfer just after it, for air we did not calculate flows for which the Rayleigh number exceeded 20000. Thus we estimate our Nusselt-number results to be accurate to about 3·5 %.

3. Results

In this section we show how the Prandtl number, the Grashof number and the aspect ratio influence the convective flow in the cavity. Most of the information is displayed in contour plots of the stream function and temperature. In all the figures the hot wall is on the left. The resulting streamlines and isotherms give the same visual information that smoke traces and interferometer fringes give in an experiment. The plots are shown undistorted by changes in the vertical scale even for the tallest cavities to give the viewer the same image as an experiment would. Results for five different Prandtl numbers were calculated. Each is discussed in turn in the following.

3.1. *Liquid metals and zero Prandtl number*

A hypothetical fluid with its Prandtl number equal to zero is one whose thermal diffusivity approaches infinity. The energy equation in this case reduces (for a bounded domain) to the steady-state conduction equation. For a rectangular slot it has the particularly simple solution of a linear temperature distribution across the slot for the boundary conditions considered. In a tall cavity the flow is parallel to the vertical sidewalls except in the end regions, the extent of which is of the order of the width of the cavity. The streamlines of this flow are shown in figure 2 (*a*). The arbitrarily large thermal diffusivity rules out thermal perturbations and the instability of the flow, which leads to multicellular convection, is purely hydrodynamic. The way in which the flow develops for increasing Grashof number is shown in figures 2 (*b–d*).

The instability for an infinitely tall cavity has been predicted (Korpela *et al.* 1973) to set in at $G = 7932$. Figure 2 (*b*) shows a weak cellular convective pattern at $G = 8000$ in a cavity of aspect ratio 15. The strongest cells are in the ends, where forced turning of the fluid by the boundary aids their development. In fact, a higher resolution in figure 2 (*a*) would reveal the end cells at $G = 5000$ when the flow is certainly stable. The effect of the ends on the cellular structure is rather unimportant, even for the last cells, judging from the way the streamlines curve. Actually a better view of this

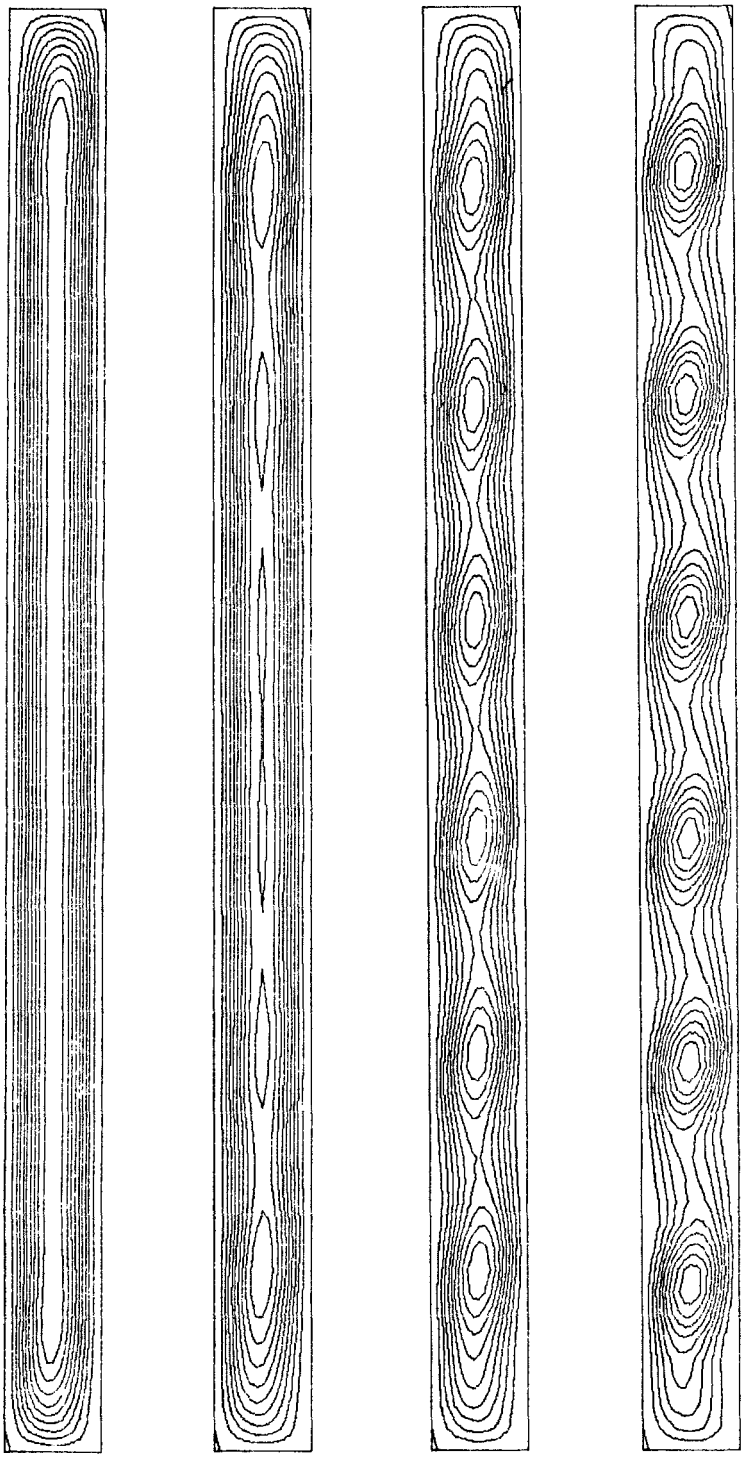

(*a*) (*b*) (*c*) (*d*)

FIGURE 2. Streamlines of flow in a cavity with $H = 15$ for a fluid with $P = 0$; (*a*) $G = 5000$; (b) 8000; (*c*) 10000; (*d*) 15000.

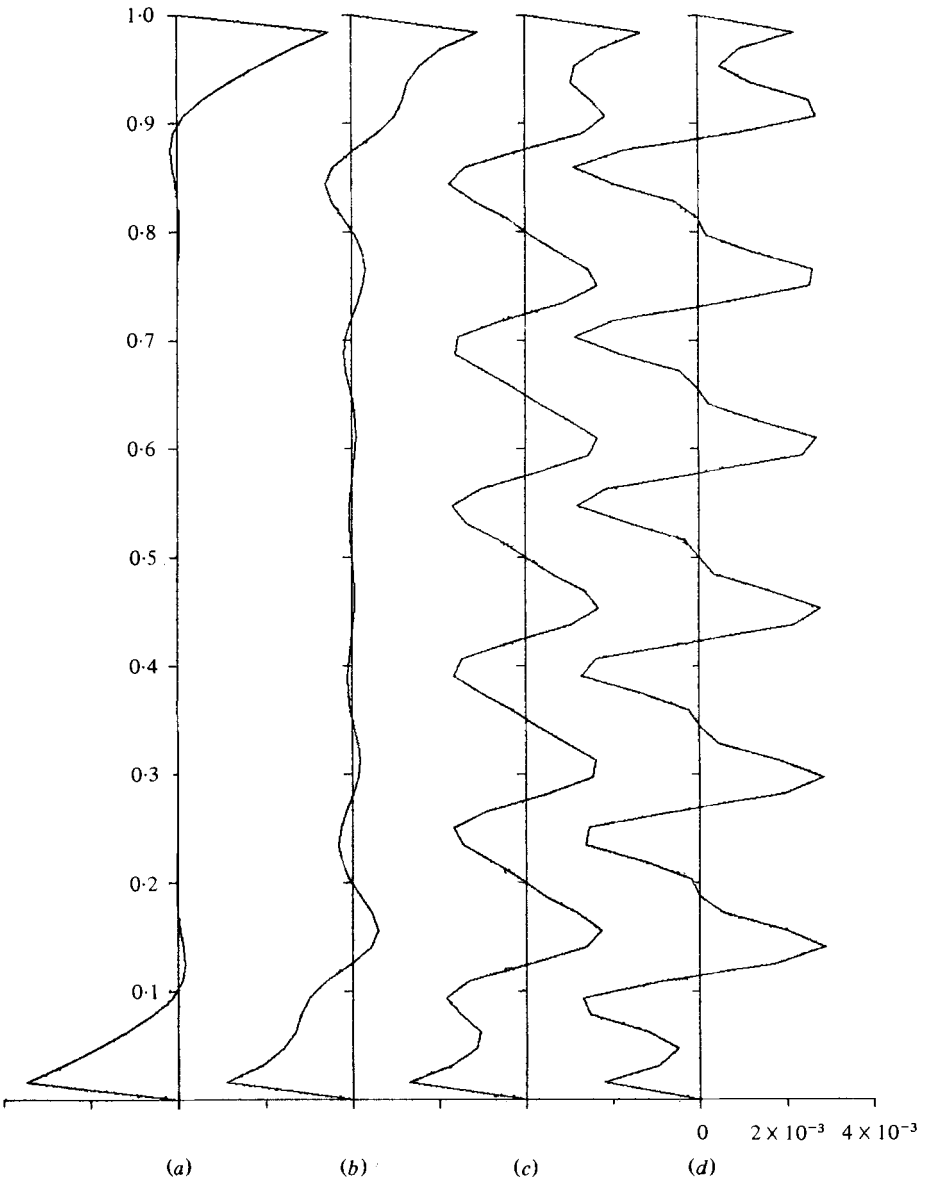

FIGURE 3. The horizontal velocity at the vertical centreline for the flow shown in figure 2. The horizontal scale markings are 2×10^{-3} apart.

can be obtained from the horizontal velocity distributions shown in figures 3(*a–d*).

Figure 3 also shows certain weaknesses in our study; namely the horizontal boundary layers in the top and bottom are not adequately resolved, and even in the centre at high values of R a finer grid ought to be used so that the jaggedness would disappear from the velocity profiles. A non-uniform grid tight in the ends would help to overcome the first problem; more computer time, the second. At the onset of instability a non-dimensional wavenumber equal to 2·69 has been predicted by linear theory of hydrodynamic stability. From figure 2 we obtain $\alpha = 2{\cdot}80$ at $G = 10000$

H \ G	8000	9000	10000	12000	15000	20000
10·0	3·05	3·01	2·93	2·86	2·82	2·77
10·5	2·78	2·76	—	2·71	2·64	—

TABLE 1. Non-dimensional wavenumbers based on the size of the two central cells for a fluid with $P = 0$. There are a total of 4 cells in the flow for all values of parameters listed.

and $\alpha = 2{\cdot}70$ at $G = 15000$. For lower values of the aspect ratio the wavenumber depends on how many cells can be fitted into a cavity of a given height. We made calculations for cavities of $H = 10$ and 10·5 and found that, when there were four cells in the cavity, the wavenumbers varied according to what is given in table 1. The wavenumbers corresponding to $H = 10$ deviate more from the predictions of the stability theory than do those for $H = 10{\cdot}5$. It did not surprise us then when we found that the flow in a cavity of $H = 10$ would also depend on the initial conditions. With the solution at $G = 8000$ as an initial condition we obtained a three-cell solution at $G = 10000$, in contrast to a solution with four cells when the Grashof number was first increased to 9000 and after that to 10000. The wavenumber of a three-cell solution is 2·26. This dependence on the initial condition was not there at $H = 10{\cdot}5$, but, as mentioned, the wavenumbers in this case were also very nearly equal to that which is favoured in an infinitely tall cavity. This non-uniqueness of the initial conditions is undoubtably present for many other values of H, but having established it for one case we did not search for it in other cases. We did not carry out any calculations for values of $R > 20000$, and so have not seen any further transitions. Thus we cannot say whether at higher values of R a transition to a periodic flow is possible in a two-dimensional flow or whether the next physically important structure is a three-dimensional steady or periodic flow.

If the Prandtl number of the fluid is increased to the range characteristic of liquid metals, very little new takes place. The same cell structure as was found for $P = 0$ develops at $P = 0{\cdot}01$ and the isotherms show only an exceedingly small periodic deviation from the vertical. The average Nusselt number is only 1·0032 at $G = 20000$ for a cavity of $H = 15$.

3.2. *Air*

In §3.1 we saw that for a fluid of $P = 0$ in a cavity with $H = 10$ there is a transition from a unicellular to a multicellular flow at $G \approx 8000$. If the fluid in the cavity were now replaced by air ($P = 0{\cdot}71$), the situation would be quite different. Instead of the flow becoming multicellular, it enters the transition regime as observed by Eckert & Carlson (1961), and, upon further increase in Grashof number, the boundary-layer regime. To see the transition to a multicellular flow one needs a cavity of larger aspect ratio. In figure 4 are shown the stream patterns for air flow in a cavity with $H = 20$. The flow patterns are similar to those for a fluid with Prandtl number zero. The transition takes place in the interval $10000 < G < 11000$. The corresponding isotherms are shown in figure 5. If the flow were thought to be in the conduction regime, use of the linear theory of hydrodynamic stability would predict it to go unstable at $G = 8038$, in substantial disagreement with our calculations and the experiments of Hollands & Koniecek (1973). The experiments show the instability to set in at $G = 11000 \pm 510$, with which our calculations agree. The reason for the discrepancy

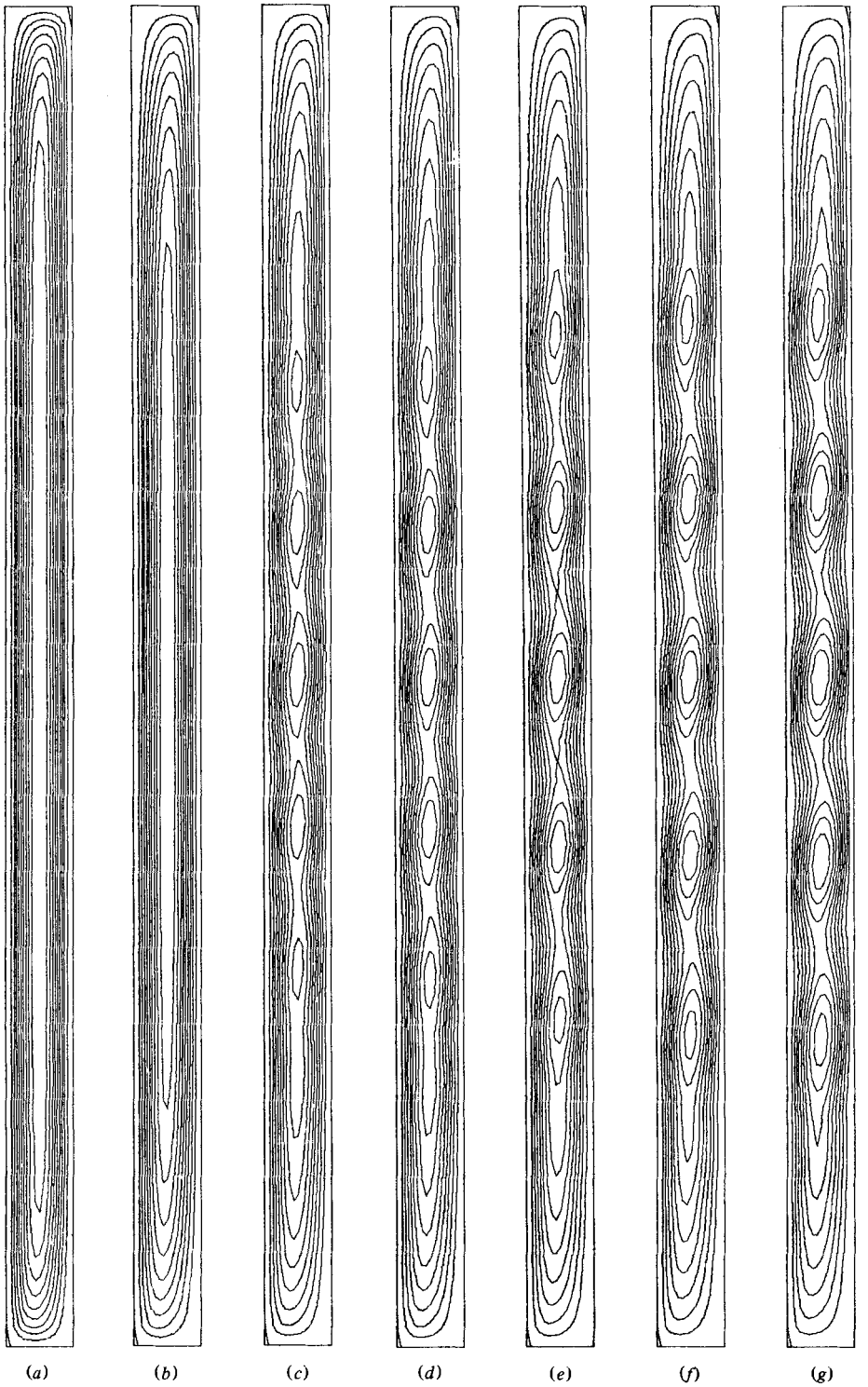

FIGURE 4. Streamlines of flow in a cavity with $H = 20$ for air as a function of Grashof number: (*a*) $G = 5000$; (*b*) 10000; (*c*) 11000; (*d*) 12000; (*e*) 15000; (*f*) 20000; (*g*) 25000.

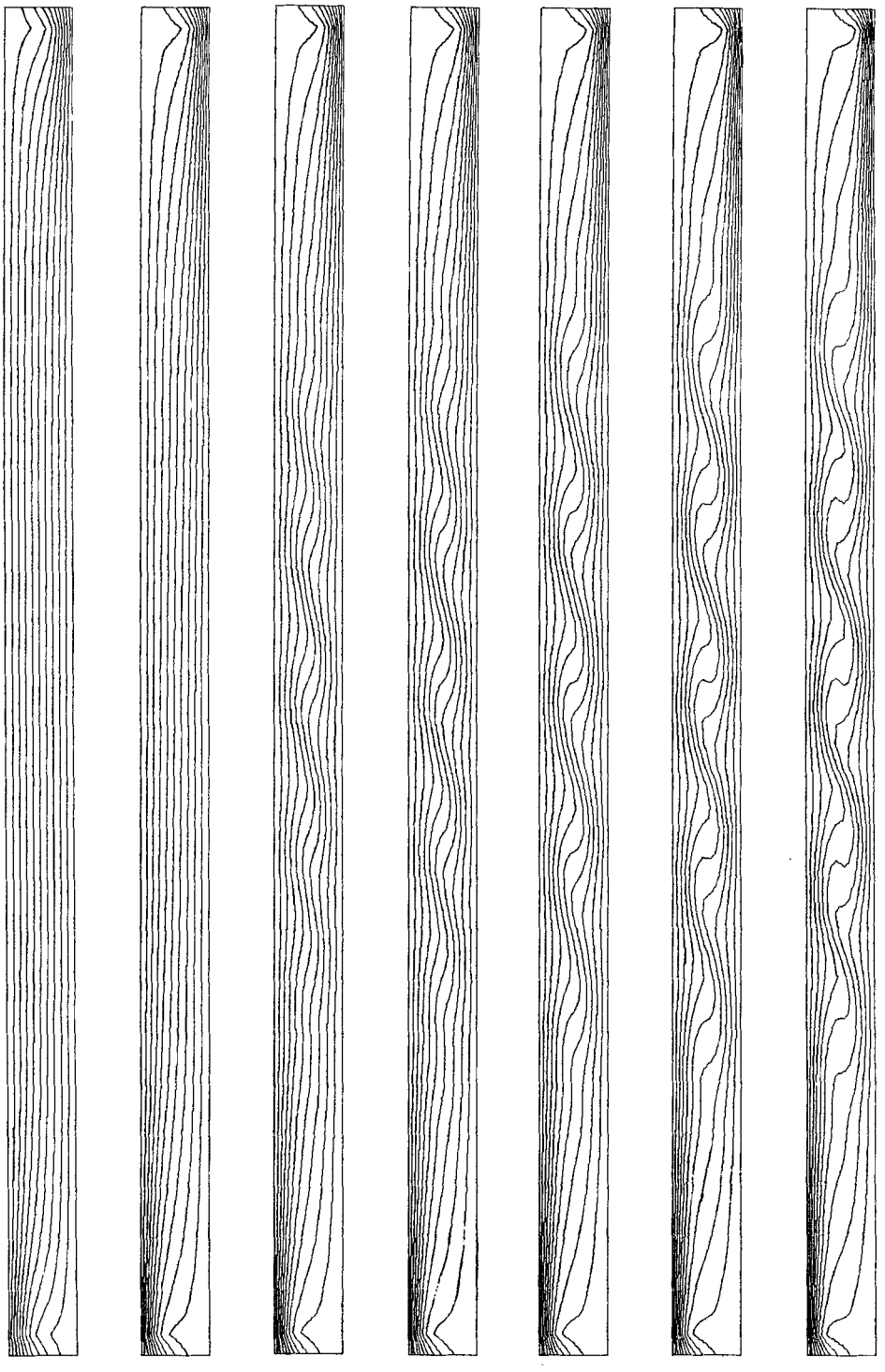

FIGURE 5. Isotherms for the flow shown in figure 4.

G	11000	12000	15000	20000	25000
$\alpha = 2\pi/\lambda$	2·82	2·78	2·50	2·41	2·33

TABLE 2. Non-dimensional wavenumbers based on the size of the central cell for air in a cavity with $H = 20$

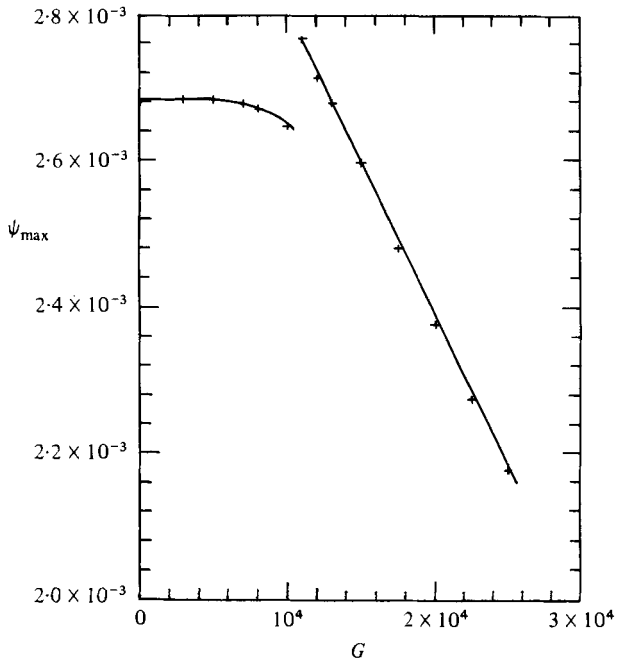

FIGURE 6. Maximum stream function at the centre of the cavity for the flow shown in figures 4 and 5.

with the theory becomes clear upon a closer examination of the isotherms in figure 5. Throughout the cavity (except in the very ends) the isotherms are inclined toward the cold wall, with the result that there is a slight vertical temperature gradient in the core. Bergholz's calculations show how much the flow is stabilized by this gradient When this is taken into account, agreement is obtained between the stability theory, the experiments and the numerical computations. The vertical temperature gradient is seen to affect also the strength of the cellular convection. In contrast with the $P = 0$ case, the cells furthest from the centre are now the weakest. The reason follows again from the fact that a vertical temperature gradient stabilizes the flow. In the ends the gradient is the strongest, and if the instability is viewed as a local phenomenon, then in the ends the departure from the onset of instability is smaller than in the centre, and hence the convection is weaker.

As the Grashof number is increased the cells become stronger and the distance between them increases. At $G = 11000$ the spacing between the centre cell and its neighbours gives 2·82 for the non-dimensional wavenumber. This decreases to 2·33 at $G = 25000$. The trend is shown in table 2. Bergholz's calculations give $\alpha = 2{\cdot}80$

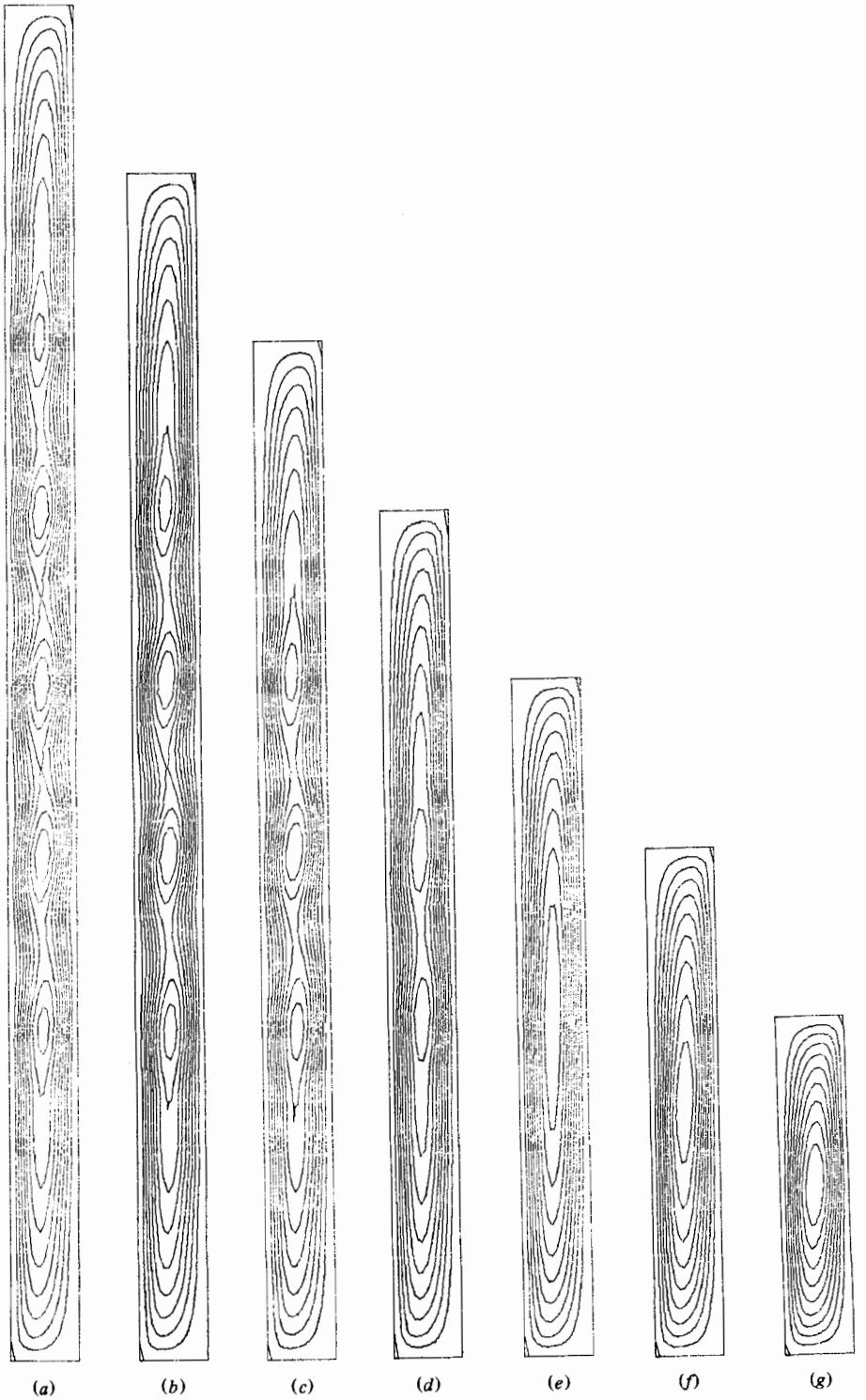

FIGURE 7. Effect of aspect ratio on convection of air at $G = 15000$: (*a*) $H = 20$; (*b*) 17·5; (*c*) 15; (*d*) 12·5; (*e*) 10; (*f*) 7·5; (*g*) 5.

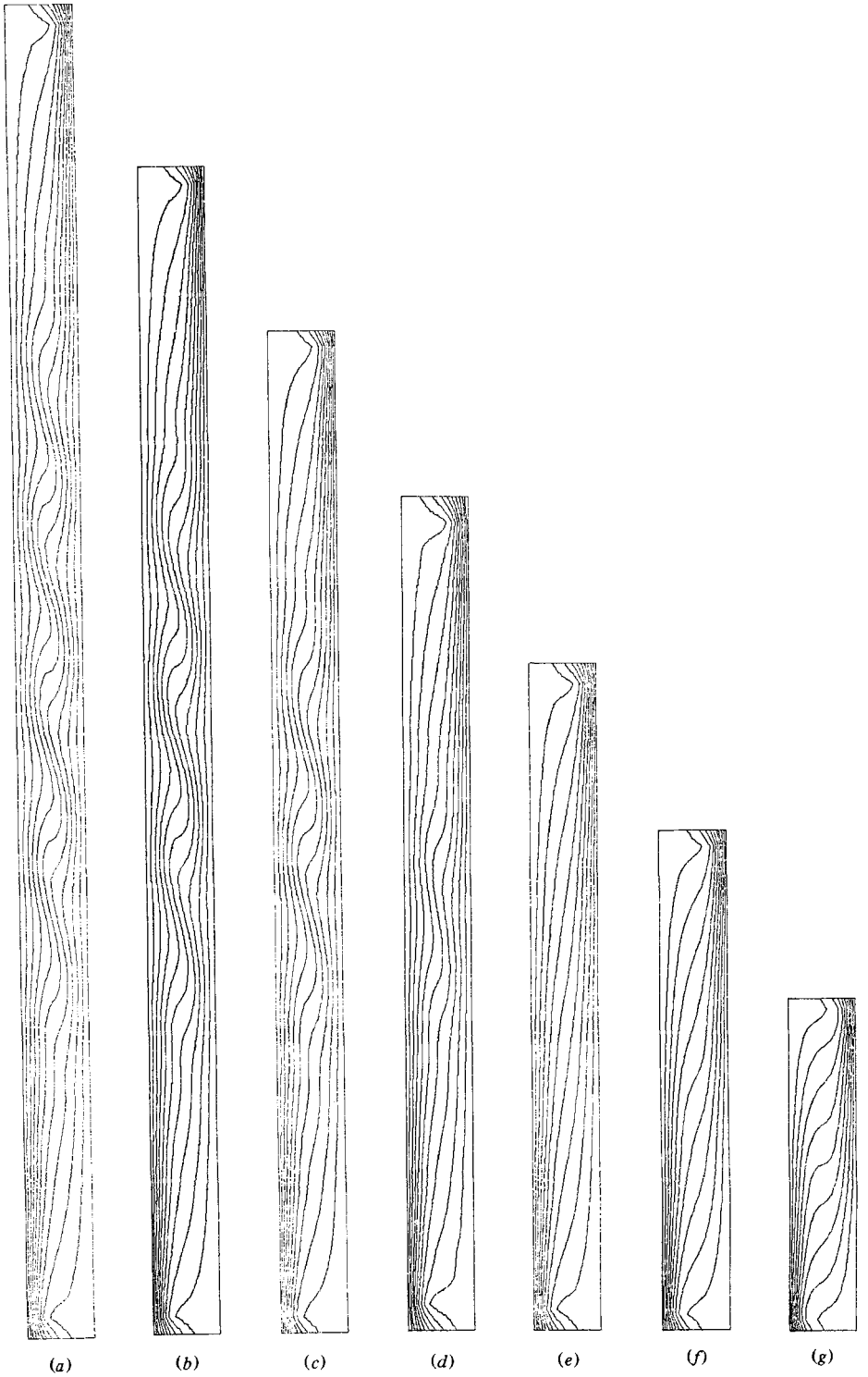

FIGURE 8. Isotherms for the flow shown in figure 7.

at the onset of instability, and the experiments of Vest & Arpaci (1969) and Korpela (1974) yield $\alpha = 2{\cdot}5 \pm 0{\cdot}2$ for a slot with $H = 33$.

When we increased the aspect ratio of the slot to $H = 40$ we obtained similar results to those at $H = 20$. The calculations were carried out on a 17×129 grid. The only notable difference was that whereas at $G = 12000$ and 15000 there were 14 cells, this number diminished by one when the Grashof number was increased to 20000 and 25000.

The maximum stream function at the centre of the cavity we have plotted in figure 6. Owing to the kind of scale used for the velocity, the stream function remains constant as the Grashof number is increased at first. As convection begins to be important, the stream function diminishes slightly and then increases sharply at the onset of instability. After the transition the flow in each of the cells is in certain ways similar to the flow in a cavity the aspect ratio of which is of the order of the wavelength of the cells. The maximum stream function now diminishes with increasing Grashof number, giving a clue to how the stream function should be scaled in an analytical attempt at the structure of the multicellular flow.

As has been noted above, a transition to multicellular flow will not take place if the aspect ratio is sufficiently small. It is of interest to establish, if only roughly, the value of the aspect ratio for which multicellular convection is first expected. From calculations such as those shown in figures 7 and 8 it is seen to be between 10 and 12·5. Lauriat (1981) obtained multicellular convection at $H = 11{\cdot}84$. The particular value of aspect ratio below which instability from the conduction regime does not take place is the result of the following. The instability is a local phenomenon determined for low-Prandtl-number fluids by the local velocity profile. The profile at the midheight of the cavity is the least stable of the family of profiles that exist in the cavity at various heights. At low values of Rayleigh number, the velocity profiles at various heights are nearly the same, and are thus equally susceptible to instability. The instability of course does not set in at small values of R. As R increases, the end regions penetrate further into the cavity, with the result that the region of potential instability gets smaller. For a cavity with $H = 10$ the end region at $R = 11000$ has penetrated into the centre before the flow becomes unstable. On the other hand, for a cavity with $H = 12{\cdot}5$ an unstable region exists at the centre at the critical value of R and a transition to multicellular flow takes place. For zero-Prandtl-number fluid there is no vertical stratification of temperature to alter the velocity profiles. As a result the multicellular convection can take place in a cavity with an aspect ratio as low as six.

There have been other calculations of convection of air reported in cavities of aspect ratios as high as 20, and even one in which it was 80 (Raithby & Wong 1981), but in most of them the transition to a multicellular flow has not been observed. The reason could well be that the numerical schemes, which rely on upwind differencing to insure numerical stability, also introduce artificial viscosity, which damps those perturbations to which the flow attempts to feed energy. This artificial damping is absent in Arakawa's method.

The stream patterns shown in figure 4 agree well with the photographs of the flow (Vest & Arpaci 1969; Korpela 1974), including the slight tilting of the cells toward the cold wall. This gives us confidence that the heat-transfer calculations to be discussed next are also reasonably accurate.

In figure 9 the vertically averaged Nusselt number $N = hL/k$ is plotted as a function of the Grashof number for cavities with H ranging from 5 to 40. In the definition of Nusselt number, h is the average heat-transfer coefficient obtained by

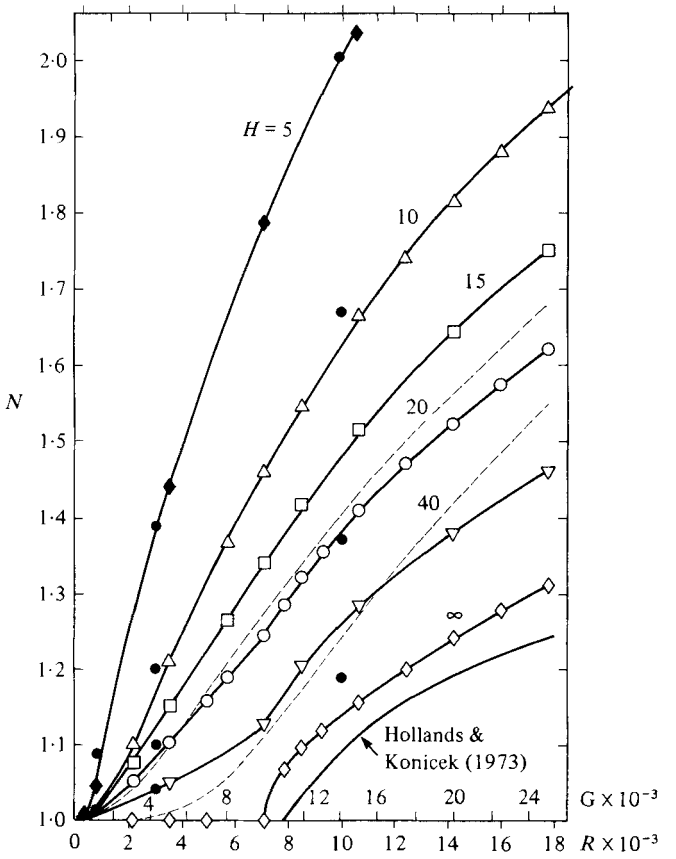

FIGURE 9. Nusselt number as a function of Grashof number for flow of air in cavities of various aspect ratios. The solid circles are calculations of Raithby & Wong (1981), the dashed lines the experiments of ElSherbiny *et al.* (1982).

averaging the heat flux over the height of the cavity and dividing the result by the temperature difference between the sidewalls. The thermal conductivity k of the fluid also appears in the definition of N. As the Nusselt number is a measure of the amplitude of the convective motion, it shows the stable branch of a bifurcated solution. To determine the contribution of multicellular convection to the average Nusselt number, we also averaged the heat transferred across the central cell and calculated from it the Nusselt number corresponding to multicellular convection in an infinitely tall cavity. The values obtained were mostly from a calculation for a cavity of $H = 20$, but the additional data from the centre cell in a cavity of $H = 40$ fall squarely on top of this, so that one can safely conclude that the data do, in fact, represent heat transfer in an infinitely tall cavity. The lowest curve in figure 9 is the experimental data of Hollands & Konicek (1973). They obtained it by averaging the heat transfer over the middle fifth of a cavity with $H = 44$. Thus the calculations and the experimental values are averaged in different ways, so that exact agreement could not be expected. The discrepancy is only about 3·5%. It could probably be reduced somewhat by a finer finite-difference mesh and extrapolation of the results to zero grid size.

Since for a sufficiently tall cavity the heat transfer across each cell no longer depends on the aspect ratio, one easily obtains an expression for the average Nusselt

G \ H	5	10	15	20	20*	40	40*	CC
3000	—	1·10	1·08	1·05	—	—	—	1·0
5000	1·44	1·21	1·15	1·11	—	1·05	—	1·0
7000	—	—	—	1·16	—	—	—	1·0
8000	—	1·37	1·26	1·19	—	—	—	—
10000	1·79	1·46	1·34	1·25	—	1·13	—	1·0
11000	—	—	—	1·29	—	—	—	1·07
12000	—	1·55	1·42	1·32	1·32	1·21	1·21	1·10
13000	—	—	—	1·35	—	—	—	1·12
15000	2·04	1·66	1·51	1·41	1·41	1·28	1·29	1·16
17500	—	1·74	—	1·47	1·47	—	1·34	1·20
20000	2·22	1·81	1·65	1·53	1·53	1·38	1·38	1·24
22500	—	1·88	—	1·58	1·58	—	1·43	1·28
25000	—	1·94	1·75	1·62	1·63	1·46	1·47	1·31

TABLE 3. Vertically averaged Nusselt numbers for air, $P = 0{\cdot}71$. The last column refers to the average Nusselt number for a centre cell in a cavity at $H = 20$. The columns with asterisks were calculated by use of (8).

number in the multicellular flow regime in which the end effect is transparent. The result is

$$N = \frac{l_b}{H} N_b + \frac{l_t}{H} N_t + \left(1 - \frac{l_b + l_t}{H}\right) N_c, \tag{7}$$

where l_b and l_t represent the non-dimensional lengths of the end regions at the top and bottom, and N_b and N_t are the respective average Nusselt numbers there. The Nusselt number for a cell is denoted by N_c. Surprisingly good agreement is obtained if we take the heat transfer across the ends to be represented by that for a cavity of aspect ratio 10. Then (7) reduces to

$$N = \frac{10}{H} N_{10} + \left(1 - \frac{10}{H}\right) N_c. \tag{8}$$

In table 3 we have included the values used to construct figure 9 as well as two columns calculated with the aid of (8) for cavities with $H = 20$ and 40. The agreement between the results calculated from this formula and those obtained from an actual calculation is seen to be very close.

Returning to figure 9, the filled circles are points calculated by Raithby & Wong (1981). For $H = 5$, two of their three points fall exactly on our line, which itself includes only 4 points. For $H = 10$ their calculations are 2·5 % higher than our curve, and at $H = 20$ our calculations agree with theirs to better than 1·5 %. At $H = 40$ for $G = 4000$ their point still agrees with our calculation, but at $G = 14000$ their Nusselt number for $H = 40$ is substantially lower. In none of their calculations did they *obtain* multicellular flow, thus the discrepancy in the last point can be attributed to this.

So far what we have presented seems to fit well together, for the explanation for the increase in the Nusselt number for the lower-aspect-ratio cavities can be considered to be the result of the energy transported across the ends. Recent experiments by ElSherbiny, Raithby & Hollands (1982) for large-aspect-ratio cavities do not fit this pattern though. These experiments were conducted with an apparatus in which the top and bottom were made of highly conducting material. Raithby & Wong (1981) have shown by calculations that this kind of end condition reduces the Nusselt number by about 5 % for a cavity of $H = 20$ in the range of

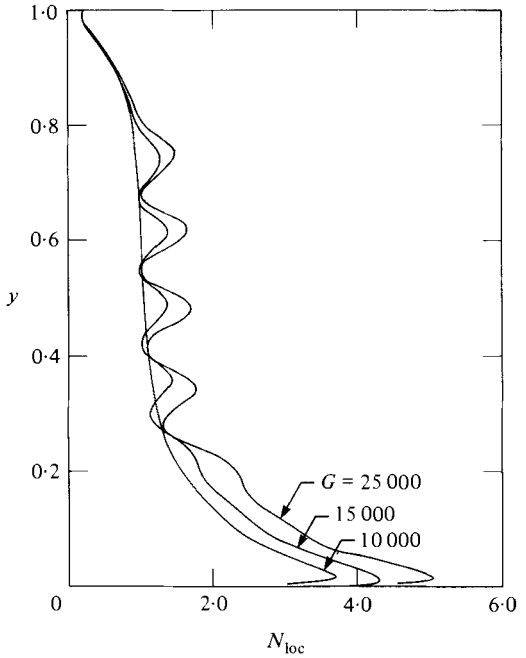

FIGURE 10. Local Nusselt numbers ($N_{loc} = h_{loc} L/k$) for air in a cavity of $H = 20$.

Rayleigh numbers of interest here, and by less for cavities of higher aspect ratio. To keep figure 9 from becoming too cluttered we have put only their experimental data for $H = 20$ and 40 into figure 9. At $H = 10$ it falls just slightly above our $H = 10$ line. But their data for $H = 80$ and 110 actually fall between the $H = 20$ and 40 lines. This is quite unexpected, and the reason for it did not become clearer to us upon further study of their paper. Their apparatus was constructed in such a way that they could measure the heat flux across each third of the vertical wall. The measurement across the central section agrees with the data of Hollands & Koniecek to better than 1·5% (this was communicated to us by Professor Raithby) and at $H = 5$ and 10 it agrees with the calculations of Raithby & Wong. However, it is hard to think of a flow in a cavity of $H = 110$ which near the bottom, where the heat flux at the hot wall is the highest, would cause the average Nusselt number at $R = 15000$ to increase from 1·2 to 1·5. Our calculations, as mentioned above, show 14 regularly spaced cells in a cavity of $H = 40$, and there is no reason to expect anything but more cells to fill a cavity of $H = 110$, and thus lead to a diminishing influence of the ends.

In figure 10 the local Nusselt numbers at the hot wall are plotted for a cavity of aspect ratio 20. The local Nusselt number is the ratio of the local heat flux to the conduction heat flux. The figure shows the increase in the Nusselt number at the centre above the conduction value of unity. This is the result of the returning cold fluid in a cell causing a crowding of the isotherms near the hot wall, which in turn leads to a higher temperature gradient in these regions.

3.3. *Water*

Bergholz (1978) has estimated that for water when H is greater than 97, multicellular convection can take place; below it the instability is of a travelling-wave type. For values of $H = 10$ and 15 our calculations show no trace of travelling waves whenever

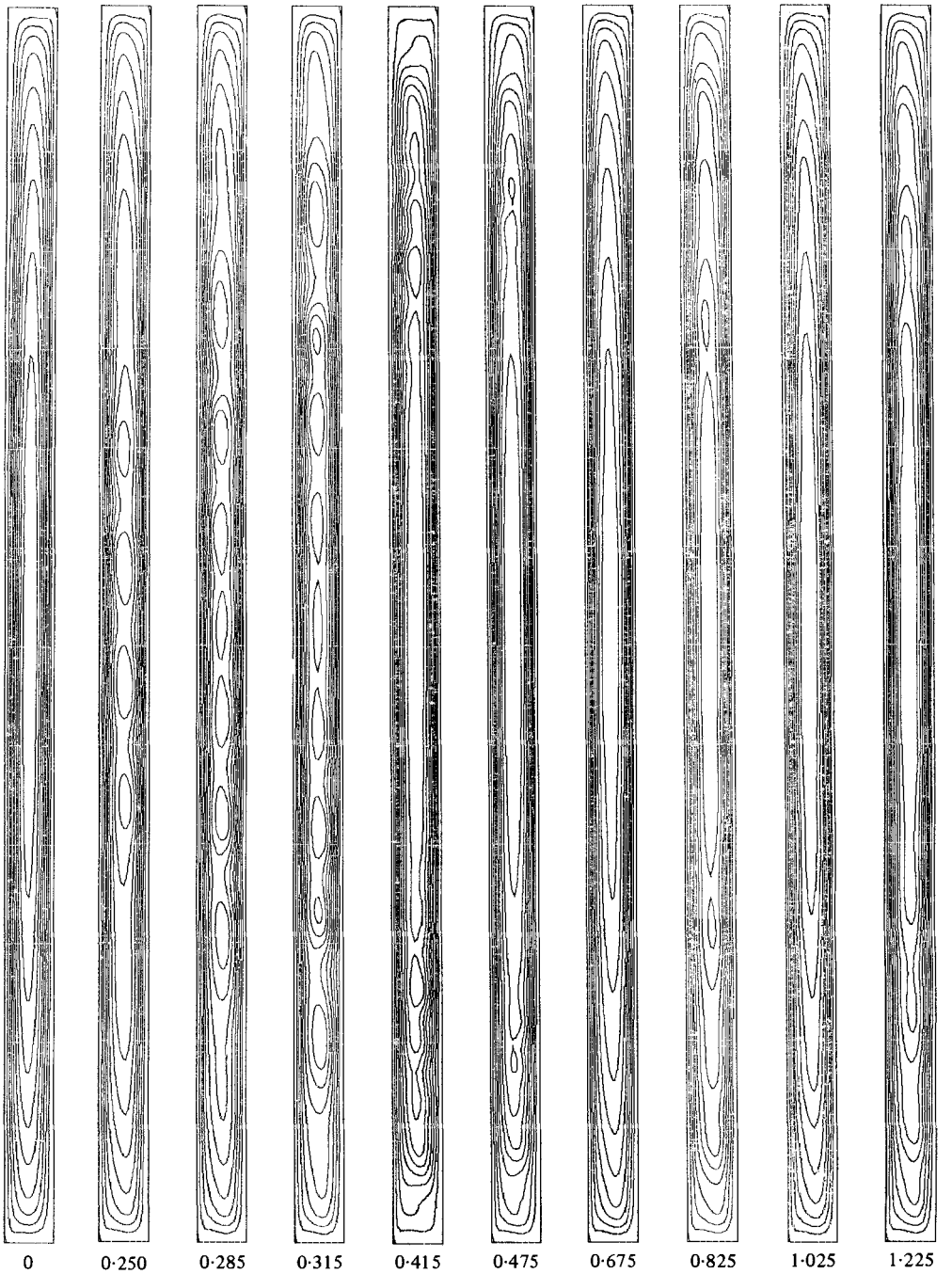

FIGURE 11(*a*). For caption see facing page.

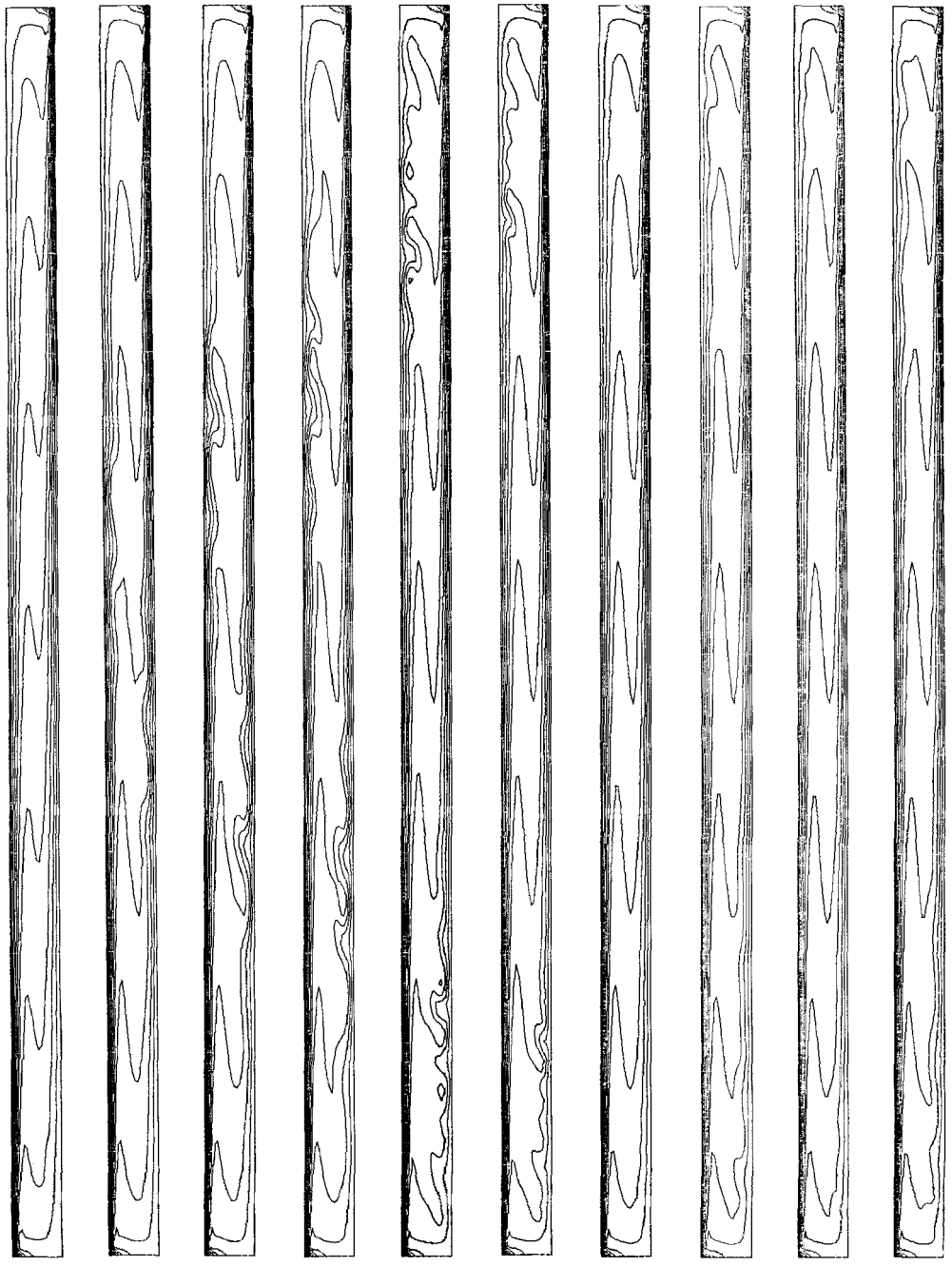

(*b*)

FIGURE 11. Time sequence of an unsteady convection of water in a cavity with $H = 25$ at $G = 40000$: (*a*) streamlines; (*b*) isotherms. The leftmost plot is the initial condition at $G = 20000$.

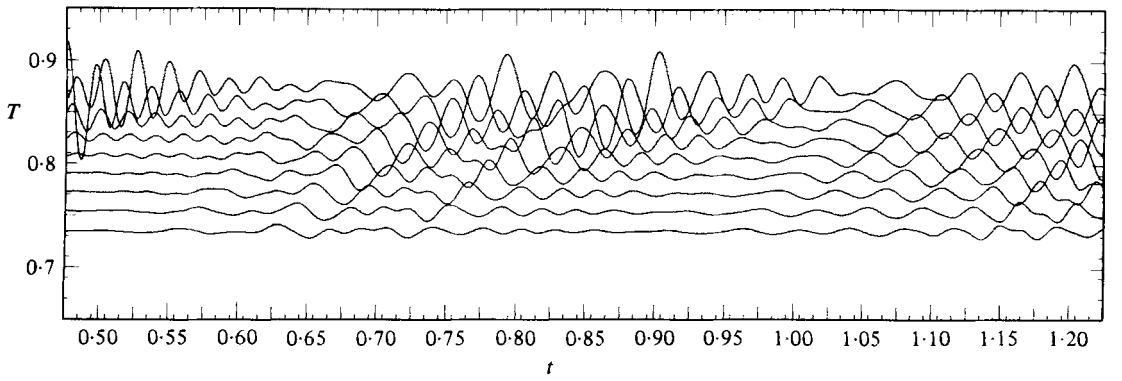

FIGURE 12. Temperature oscillations at $x = 0{\cdot}1$ and at equidistant intervals between $y = 0{\cdot}5$ for the lowest curve and $y = 0{\cdot}875$ for the highest.

$0 \leqslant G \leqslant 40000$. For $H = 25$ Hart (1971) observed the travelling-wave instability to set in at $G = 19400 \pm 1100$, and Bergholtz (1978) predicted that it would appear at $G = 12000$. Our numerical results for this case, obtained with a 21×129 grid, are shown in figures 11 (a, b). The entire calculation took 27·7 minutes of central-processor time. The first plot on the left is nearly steady flow at $G = 20000$. The flow actually never reached steady state but contained small fluctuations in the flow variables. With this as an initial condition we increased the Grashof number to 40000 and calculated the transient solution. The time step was 5×10^{-4}. At $t = 0{\cdot}25$ four cells are apparent in the central portion of the cavity. The cells move upward in the upper half of the cavity and downward in the lower half. While they drift towards the ends additional cells are formed at the centre. By the time $t = 0{\cdot}415$ the cellular structure at the centre has disappeared and only a couple of cells are left in the ends. Shortly after this the transient is over. The flow does not become steady, however, but remains quasi-periodic. This is evident from the waviness of the isotherms in figure 11 (b). In figure 12 we show it more clearly by plotting the fluctuations of the temperature at nine locations near the hot wall of the cavity. All of them are a distance equal to one-tenth of the cavity width away from the wall. The lowest curve gives the trace of the temperature oscillation at $y = 0{\cdot}5$, the midheight of the slot, and the top one at $y = 0{\cdot}875$. The rest are at equidistant intervals in between. From these traces we calculated the wave speed and compared it with the maximum vertical velocity. At $y = 0{\cdot}5$ the non-dimensional wave speed is $2{\cdot}2 \times 10^{-3}$, whereas the largest vertical velocity is $2{\cdot}3 \times 10^{-3}$. At $y = 0{\cdot}875$ the corresponding numbers are $3{\cdot}2 \times 10^{-3}$ and $1{\cdot}5 \times 10^{-3}$. It is known that for instability of travelling-wave type the wave speed is often close to the maximum velocity of the base flow. Thus our calculations measure up favourably on this account and they are also of the same order in magnitude as the critical wave speeds predicted by Bergholz (1978).

3.4. *Fluids of large Prandtl number*

For fluids whose Prandtl number is larger than 12·7 the instability from the conduction regime sets in as a travelling wave. But this can only be observed in very tall cavities. In a moderately high cavity, as the Grashof number is increased the flow will enter the transition and boundary-layer regimes before the instability from the conduction regime occurs. In figures 13 and 14 we show plots of streamlines and isotherms for a flow of a fluid with $P = 20$ in a cavity with $H = 15$. For the

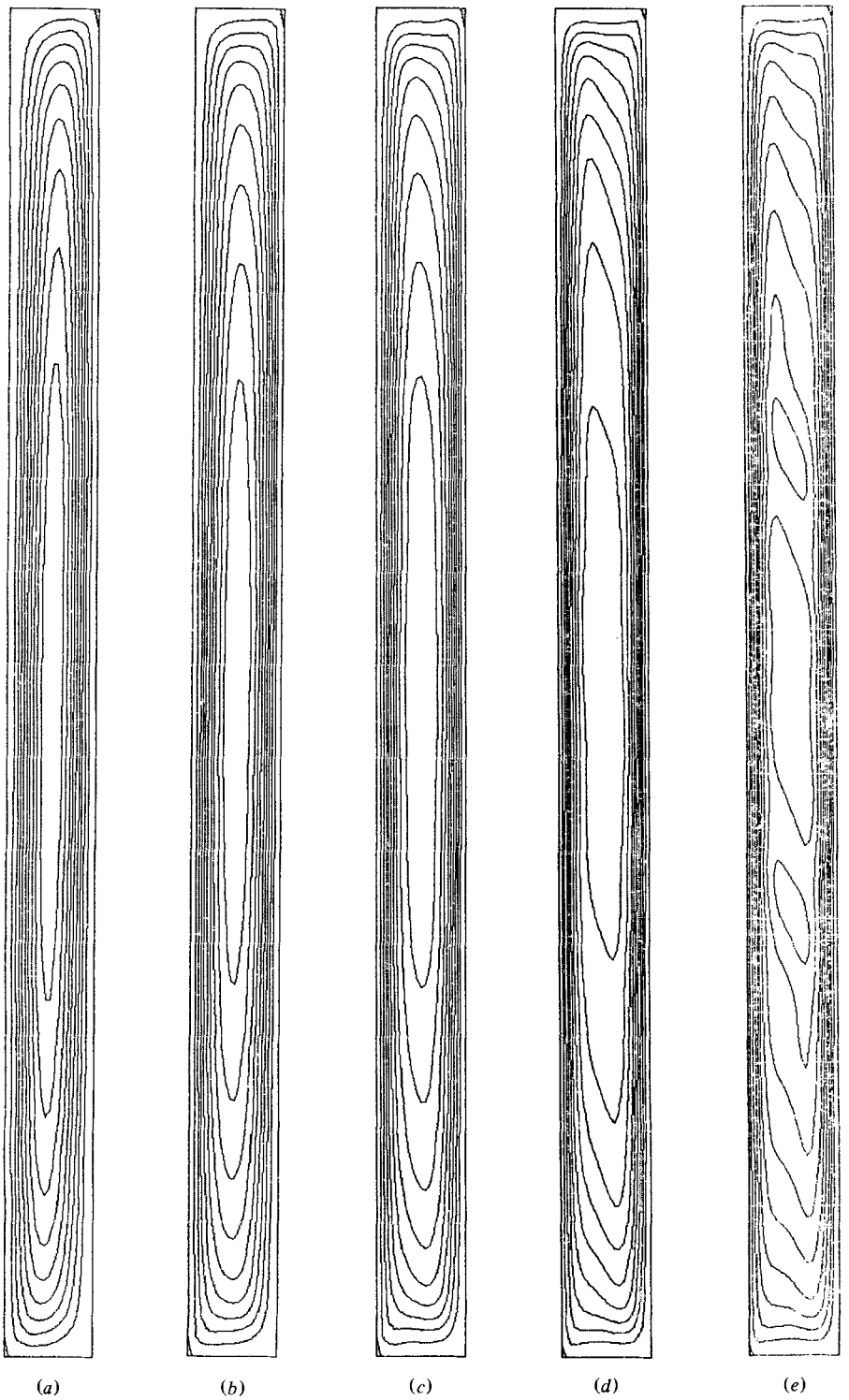

FIGURE 13. Streamlines for convection of a fluid with $P = 20$ in a cavity of aspect ratio $H = 15$: (*a*) $G = 1000$; (*b*) 5000; (*c*) 10000; (*d*) 20000; (*e*) 30000.

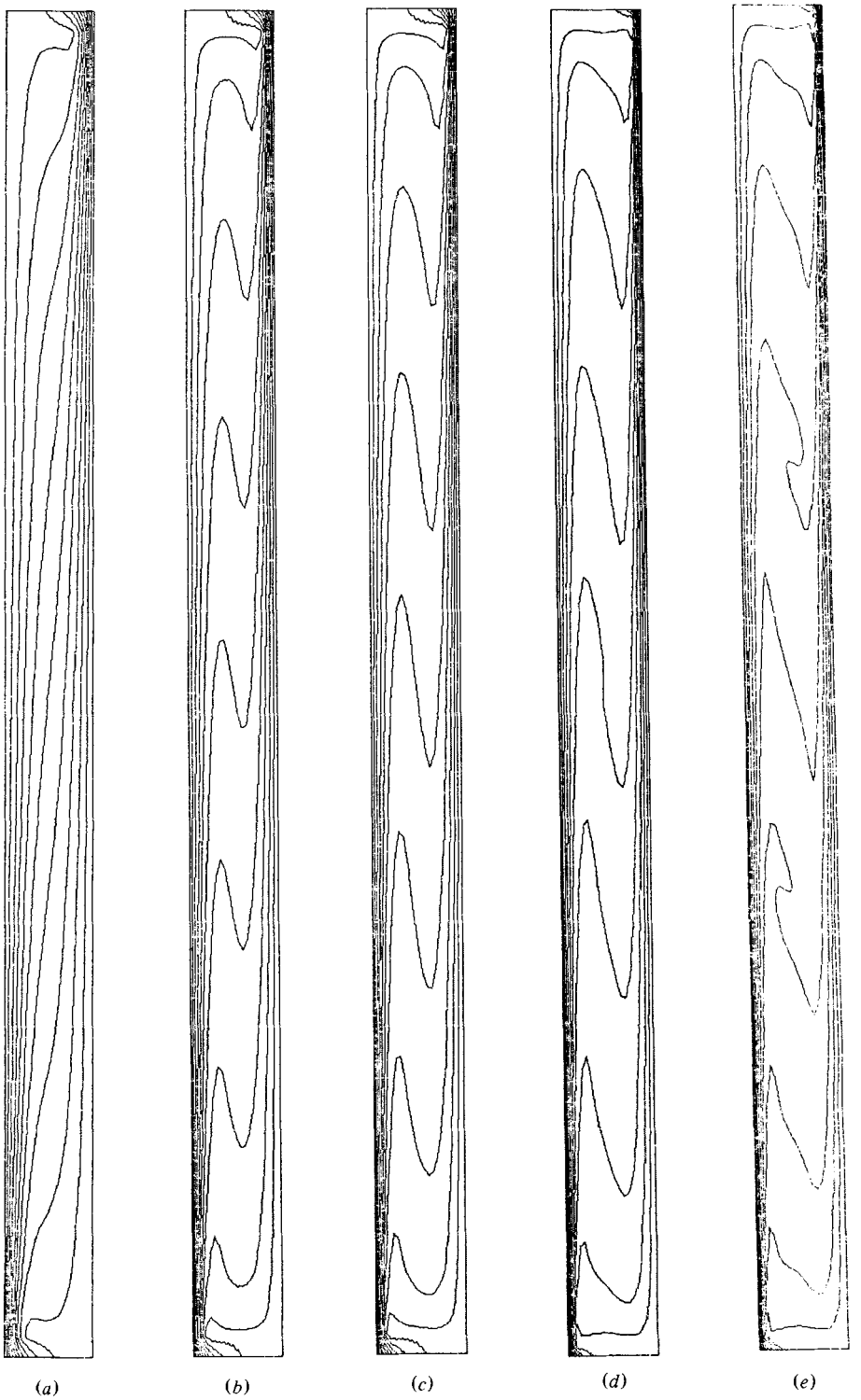

FIGURE 14. Isotherms for the flow in figure 13.

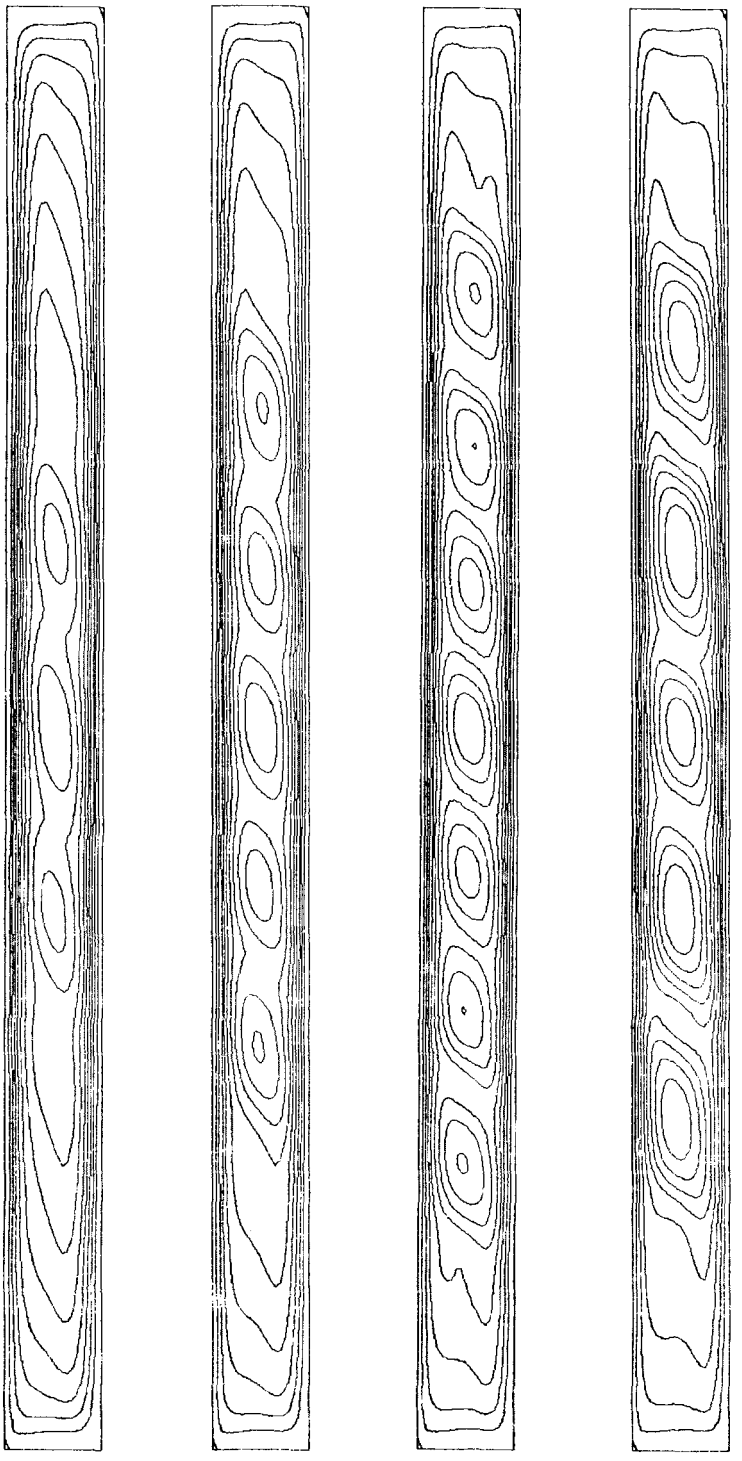

FIGURE 15. Streamlines for convection of an oil with $P = 1000$ in a cavity of aspect ratio $H = 15$: (*a*) $G = 400$; (*b*) 600; (*c*) 1000: (*d*) 1500.

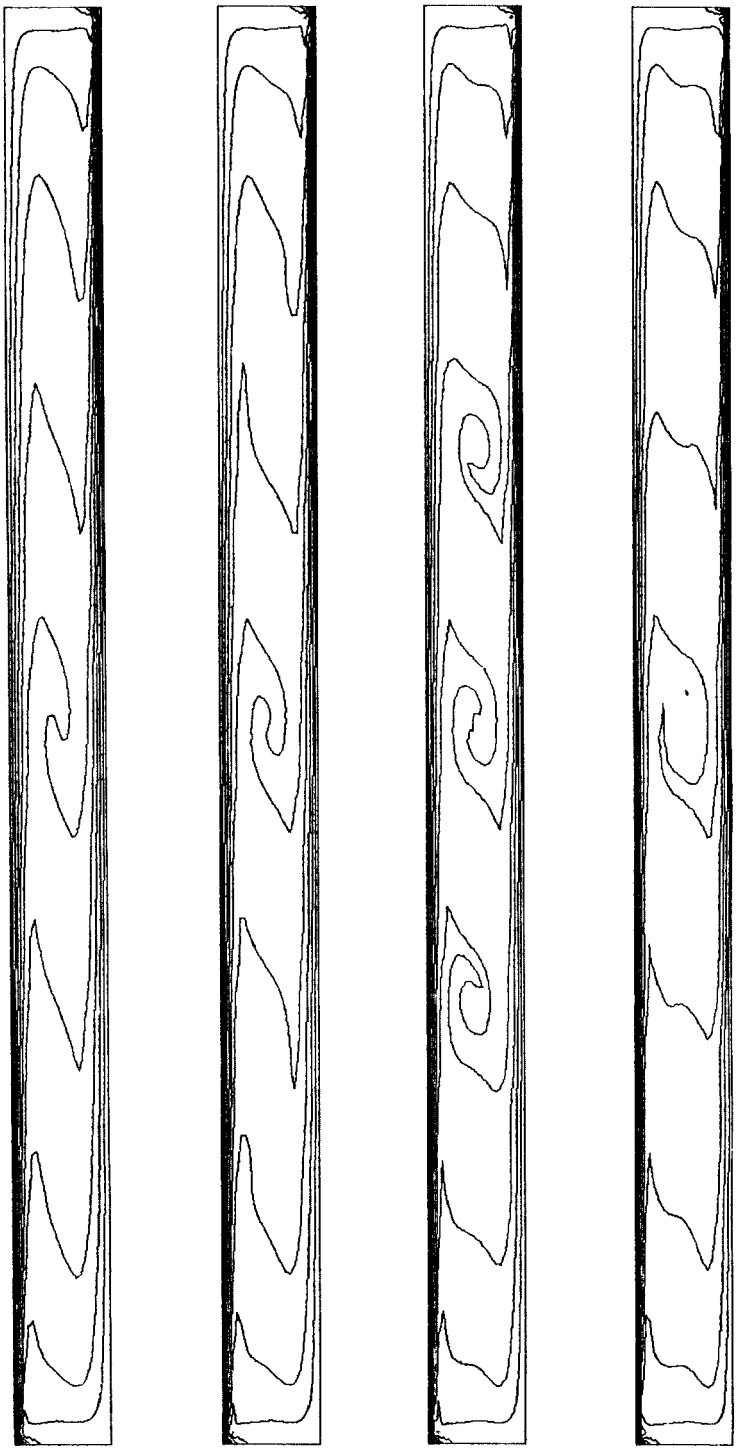

(*a*) (*b*) (*c*) (*d*)

FIGURE 16. Isotherms for the flow in figure 15.

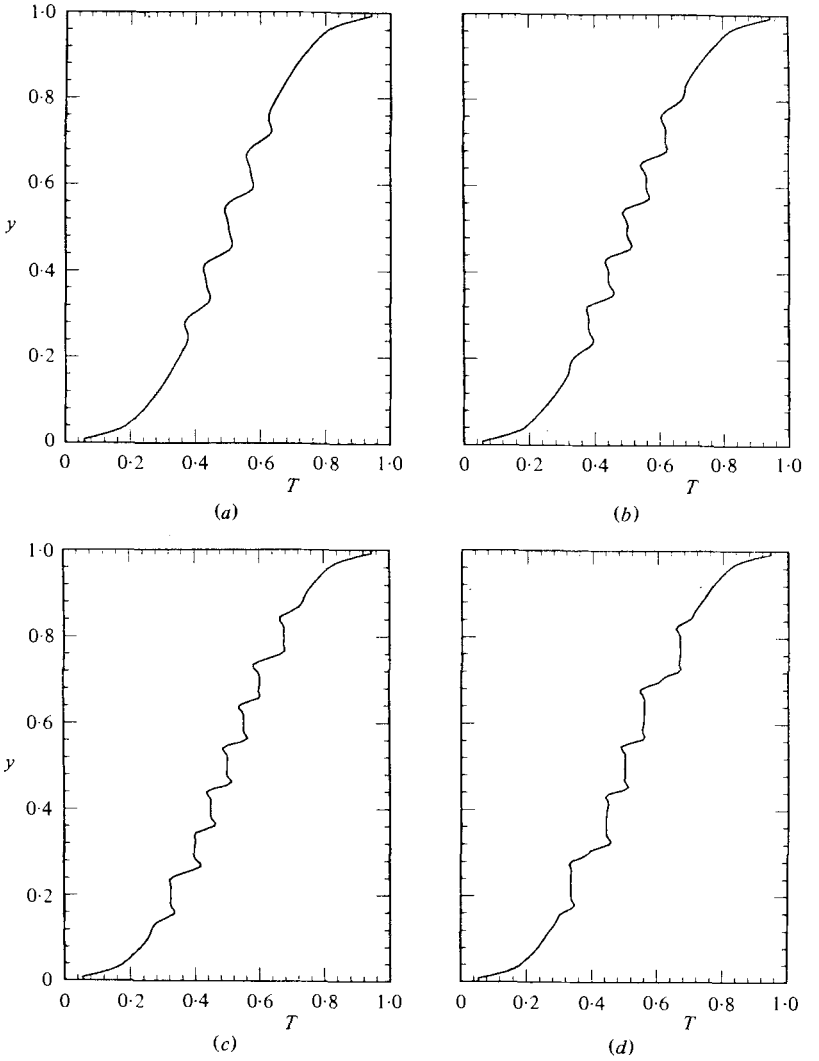

FIGURE 17. Temperature along a vertical centreline for convection of an oil with $P = 1000$ in a cavity of aspect ratio $H = 15$. The values of G are (*a*) 400; (*b*) 600; (*c*) 1000; (*d*) 1500.

calculations for which $G = 1000$, 5000 and 10000 we used a 21×65 grid, and refined it to a 21×129 grid when G was 20000 and 30000. At $G = 1000$ the flow is already in the transition regime. The boundary-layer regime is encountered for values of G equal to 5000 and higher. Characteristic of these flow regimes is the vertical temperature gradient in the core. We give it the symbol S. Its value at the centre is 0·56 at $G = 5000$ and for $G = 10000$ it is 0·51. These two values agree with Elder's (1965) experimental values for high-Prandtl-number fluids. To relate our calculations to Bergholz's (1978) predictions for the onset of instability we must calculate a scaled version of the vertical temperature stratification. It is given by the expression $\gamma = (0{\cdot}25RS/H)^{\frac{1}{4}}$. By taking $S = 0{\cdot}5$ the values for γ at $G = 5000$, 10000 and 20000 become 5·37, 6·39 and 7·60 respectively. The states corresponding to these sets of parameters are above the critical curve for the travelling-wave mode but below the critical curve for the stationary mode. Thus the flow ought to show a travelling-wave

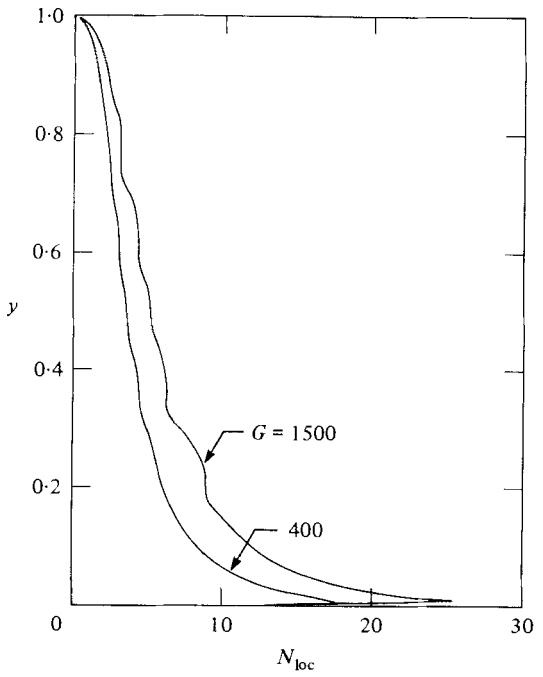

FIGURE 18. Local Nusselt numbers for oil of $P = 1000$ in a cavity of $H = 15$.

instability. It does not. Two reasons to explain the disagreement come to mind. First there is enough uncertainty in the form of the base flow used in the stability analysis that the actual flow may in fact be stable as the numerical solution shows. Equally well, the amplification rate could be so small that in the numerical solution the disturbances are not able to develop sufficiently to be observed. We don't know what the right reason for the disagreement is.

The rightmost plots in figures 13 and 14 correspond to $G = 30000$ and $\gamma = 8{\cdot}41$. These values place the state of the flow above the critical curve for the stationary mode, and indeed the numerical results show that a transition to a stationary multicellular flow has taken place.

As a final set of results we present calculations for a fluid with $P = 1000$. This is sufficiently high value to make the results insensitive to even large variations in the Prandtl number. The pertinent experimental observations to which the numerical solution can be compared consist of the original experiments by Elder (1965), those of Vest & Arpaci (1969) and the more recent results of Seki *et al.* (1978), Actually we are here covering old ground, for successful numerical calculations of high-Prandtl-number flows have been already reported in this journal by de Vahl Davis & Mallinson (1975) and Seki *et al.* (1978). Nevertheless we judge it significant that, unlike the methods used by others, the numerical technique we have employed gives believable results for all values of the Prandtl number. Our results for $P = 1000$ are shown in figures 15 and 16. They were again obtained on a 21×129 grid. For his experiments Elder determined the transition to a multicellular flow to take place at $G = 330 \pm 30\,\%$ and Vest & Arpaci concluded that in their case the corresponding number is $411 \pm 10\,\%$. Their fluid had $P = 900$. Assuming that the vertical temperature gradient is again about 0·5, the stratification factor in Elder's study, which had

$H = 19$, comes out to be 6·83. For Vest & Arpaci, who had a slot with $H = 20$, the corresponding number is 6·93. Both of these are slightly above the critical curve calculated by Bergholz. In our calculations we find at $G = 400$ weak cellular motions in the central region. Since our aspect ratio is only 15 our stratification factor comes out to be 7·6. For this value of γ Bergholz predicts a critical Grashof number equal to 240. So we are well above it. The shape and orientation of the cells is in good agreement with experimental observations. As the Grashof number is increased, the circulation in the secondary cells becomes stronger and the number of waves in the cavity increases first from three to seven, and then two pairs of them combine leading to a five cell pattern at $G = 1500$. The isotherms of figure 16 show a rather thin thermal boundary layer in the vertical sidewalls. For 21 grids across the cavity the estimate of Gill (1966) for the boundary-layer thickness, viz $\delta/L = 1{\cdot}8(H/Ra)^{\frac{1}{4}}$, puts only 2 grid points inside the boundary layer. We believe nevertheless that our results are qualitatively correct, as they are similar to what has been observed in experiments.

A different view of the thermal structure is provided by figure 17, in which the temperature is plotted along a vertical centreline of the cavity. At the two highest values of Grashof number the temperature in the core of a cell is seen to be constant with a slight overshoot at the boundaries of the cells. The background vertical temperature gradient is not affected by the cells and remains at 0·5. The contribution of the thermal energy transfer by the cells is nil. The local Nusselt numbers in figure 18 show only slight waviness where the cells are. The same conclusion was drawn by Seki *et al.* based on their experiments.

4. Final comments

The aim of this study was to calculate the multicellular flow patterns observed in laboratory experiments of natural convection in tall vertical enclosures. We were able to carry this out for fluids with Prandtl numbers ranging from zero to 1000. Except for the case when the Prandtl number is thousand, the results are new. Other attempts at calculating these flows are likely to have suffered from too much damping in the finite-difference method used. We attribute our success to the Arakawa differencing of the Jacobian. That this method works well has of course been known to meteorologists for a long time already. This study is further affirmation of it. Calculations for low Prandtl numbers can be done quite rapidly. At high Prandtl numbers they are slowed because of unsteadiness in the flow. The cells do not settle down into their final positions as fast as they do for flows of low-Prandtl-number fluids. This unsteadiness and restriction on the Courant number, both of which lead to long computer runs for high values of Grashof number, prevented us from exploring how the multicellular structure might evolve further. We are considering taking it up later when powerful computers such as the Cray become common property in educational institutions, or when we gain access to one of the existing ones.

We have shown in this article that those flow features that have been seen in experiments and have been predicted by stability theory can be obtained by numerical calculations. To get still better agreement with experiments the temperature dependence of the fluid properties should be incorporated into the equations. Equally important is for an experimentalist to consider how the idealized situation of constant-temperature sidewalls and insulated ends can be obtained to high accuracy in practice. The high local heat transfer near the bottom of the hot wall and near the top of the cold wall can cause local non-uniformities in the wall

temperature in these regions. This may lead to unaccounted-for discrepancies in making comparisons between the theory and experiments.

We wish to acknowledge the Heat Transfer Program of the National Science Foundation through Grant 76-18426 for providing funds, and the Instructional and Research Computer Center of The Ohio State University for providing computer time to carry out this study.

REFERENCES

ARAKAWA, A. 1966 *J. Comp. Phys.* **1**, 119.

BATCHELOR, G. K. 1954 *Q. Appl. Math.* **12**, 209.

BEJAN, A. 1979 *J. Fluid Mech.* **90**, 561.

BERGHOLZ, R. F. 1978 *J. Fluid Mech.* **84**, 743.

BIRIKH, R. V., GERSHUNI, G. Z., ZHUKHOVITSKII, E. M. & RUDAKOV, R. N. 1972 *Prikl. Math. Mekh.* **36**, 745.

BUNEMAN, O. 1969 *SUIPR Rep.* no. 294, *Institute of Plasma Research, Stanford University.*

CHOI, I. G. & KORPELA, S. A. 1980 *J. Fluid Mech.* **99**, 725.

CHU, H. N. S. & CHURCHILL, S. W. 1977 *Comp. & Chem. Engng* **1**, 103.

DUFORT, E. C. & FRANKEL, S. P. 1953 *Math. Tables & Other Aids to Comp.* **7**, 135.

ECKERT, E. R. G. & CARLSON, W. O. 1961 *Int. J. Heat Mass Trans.* **2**, 106.

ELDER, J. W. 1965 *J. Fluid Mech.* **23**, 77.

ELDER, J. W. 1966 *J. Fluid Mech.* **24**, 823.

ELSHERBINY, S. M., RAITHBY, G. D. & HOLLANDS, K. G. T. 1982 *Trans. A.S.M.E.* C: *J. Heat Transfer* **104**, 96.

FESTA, J. F. 1970 Thesis, Massachusetts Institute of Technology.

GERSHUNI, G. Z. 1953 *Zh. Tech. Fiz.* **23**, 1838.

GILL, A. E. 1966 *J. Fluid Mech.* **26**, 515.

GILL, A. E. & DAVEY, A. 1969 *J. Fluid Mech.* **35**, 775.

GILL, A. E. & KIRKHAM, C. C. 1970 *J. Fluid Mech.* **42**, 125.

GRAEBEL, W. P. 1980 *Int. J. Heat Mass Trans.* **24**, 125.

GRONDIN, J. C. & ROUX, B. 1979 *Rev. Phys. Appl.* **14**, 49.

HART, J. 1971 *J. Fluid Mech.* **47**, 547.

HOLLANDS, K. G. T. & KONICEK, L. 1973 *Int. J. Heat Mass Transfer* **16**, 1467.

HORNE, R. N. & SULLIVAN, M. J. 1974 *J. Fluid Mech.* **66**, 339.

KORPELA, S. A., GÖZUM, D. & BAXI, C. B. 1973 *Int. J. Heat Mass Transfer* **16**, 1683.

KORPELA, S. A. 1974 *Int. J. Heat Mass Transfer* **17**, 215.

KÜBLBECK, K., MERKER, G. P. & STRAUB, J. 1980 *Int. J. Heat Mass Transfer* **23**, 203.

LEE, Y., KORPELA, S. A. & HORNE, R. N. 1982 In *Proc. 7th Int. Heat Transfer Conf., Munich* vol. 2, p. 221.

LAURIAT, G. 1980 *A.S.M.E. Paper* 80-HT-90.

MALLINSON, G. D. & VAHL DAVIS, G. DE 1973 *J. Comp. Phys.* **12**, 435.

MALLINSON, G. D. & VAHL DAVIS, G. DE 1977 *J. Fluid Mech.* **83**, 1.

MORRISON, G. L. & TRAN, V. Q. 1978 *Int. J. Heat Mass Transfer*, **21**, 203.

NEWELL, M. E. & SCHMIDT, F. W. 1970 *Trans. A.S.M.E.* C: *J. Heat Transfer*, **92**, 159.

OZOE, H. 1976 Ph.D. dissertation, Kyoto University.

OZOE, H., OKAMOTO, T., CHURCHILL, S. W. & SAYAMA, H. 1978 In *Proc. 6th Heat Transfer Conf., Toronto*, vol. 2, p. 293.

PEPPER, D. A. & HARRIS, S. D. 1977 *Trans. A.S.M.E.* I: *J. Fluids Engng* **99**, 649.

QUON, C. 1972 *Phys. Fluids* **15**, 12.

QUON, C., 1977 *Trans. A.S.M.E.* C: *J. Heat Transfer* **99**, 340.
RAITHBY, G. D. & WONG, H. H. 1981 *Number Heat Transfer* **4**, 447.
ROACHE, P. J. 1972 *Computational Fluid Dynamics.* Hermosa.
ROUX, B., GRONDIN, J. C., BONTOUX, P. & GILLY, B. 1978 *Numer. Heat Trans.* **1**, 331.
RUBEL, A. & LANDIS, F. 1969 *Phys. Fluids Suppl. II* **12**, II-208.
RUDAKOV, R. N. 1967 *Prikl. Mat. Mekh.* **31**, 376.
RUTH, D. 1979 *Int. J. Heat Mass Transfer* **22**, 1199.
SCHINKEL, W. M. M. 1980 Ph.D. dissertation, Dept of Applied Physics, Delft University.
SEKI, N., FUKUSAKO, S. & INABA, H. 1978 *J. Fluid Mech.* **84**, 695.
THOM, A. 1933 *Proc. R. Soc. Lond.* A **141**, 651.
THOMAS, R. W. & VAHL DAVIS, G. DE 1970 In *Proc. 4th Int. Heat Transfer Conf., Paris*, NC2.4.
VAHL DAVIS, G. DE 1968 *Int. J. Heat Mass Transfer* **11**, 1675.
VAHL DAVIS, G. DE & MALLINSON, G. D. 1975 *J. Fluid Mech.* **72**, 87.
VEST, C. M. & ARPACI, V. S. 1969 *J. Fluid Mech.* **36**, 1.
WILKES, J. O. & CHURCHILL, S. W. 1966 *A.I.Ch.E. J.* **12**, 161.
WIRTZ, R. A. & LIU, L. H. 1975 *Int. J. Heat Mass Transfer* **18**, 1299.